Chapter 2

Sample Selection

2.1 Cluster selection

There are multiple reasons for choosing clusters of galaxies as the preferred target for FP work. Clusters are the most common solution to the problem of obtaining a FP (or TF) template, because a cluster sample is composed of objects that are effectively all at the same distance from the observer, and their relative fluxes and diameters are not affected by peculiar velocities, unlike those of field galaxies. The uncertainty which characterizes FP and TF distance estimates for single objects is large enough to require averages taken over $\sim$10 objects before any significant comparison can be made. This kind of average can be obtained using either rather large volumes and the sparse field population within those volumes (typical choice is to use cubic cells 5 to 10 Mpc on a side), or clusters of galaxies and the large number of objects that a cluster sample can provide. Because of morphological segregation, the early-type galaxies that are the target of FP works are found preferentially within rich clusters. The existing correlation between cluster richness and the properties of the intracluster medium (ICM) provides the opportunity to perform the TF–FP comparison under different environmental conditions. Since it is most likely for the ICM to play a significant role in any mechanism responsible for a non universality of the TF and FP relations, different cluster environments should provide a very effective test for TF and FP universality.

In a recent work Giovanelli *et al.* (1997a,b hereafter G97a, G97b) have obtained TF measurements for a large sample of cluster objects ($\simeq$ 750 galaxies in 24 clusters). It was therefore an obvious decision to select a subset of these clusters as the target for this FP work. Because one of the main goals of G97b was to obtain a kinematical rest frame that could then be used to study the local peculiar velocity field, it was important that their sample had a rather uniform sky coverage, so that localized anomalies in the velocity field would average out in the global sample. The main goal of this work is a detailed, point-by-point comparison of distance estimates, irrespective of the possible peculiar velocities that the target clusters might have. Therefore a uniform sky coverage is not important here, and the only important aspect of the sample selection is to obtain a wide spread in cluster richness and the properties of the ICM.

The sample is therefore composed of 8 clusters and rich groups of galaxies: Coma (a1656), A2634, A1367, A262, Pegasus, Cancer, NGC 507 group, NGC 383 group. Table 2.1 lists the most important properties of these clusters.

Table 2.1 Clusters and Groups properties

Name	R.A. (1950)	Dec (1950)	V_{hel}	V_{CMB}	σ	L_X[a] ergs s^{-1}	T_g keV	HI def %
			— km s^{-1}—					
N383	01 04 39.4	+32 08 46	5161	4865	553	$<2.0\ 10^{42}$	–	10[b]
N507	01 20 51.1	+32 59 40	5091	4808	643	$<2.0\ 10^{42}$	–	10
A262	01 49 49.9	+35 54 21	4896	4642	462	$2.63\ 10^{43}$	2.4	48
Cancer[c]	08 17 40.7	+21 13 36	4705	4939	317	$<2.0\ 10^{42}$	–	21
A1367	11 41 57.0	+20 03 30	6408	6735	822	$7.01\ 10^{43}$	3.7	42
Coma	12 57 11.1	+28 13 48	6917	7185	1010	$6.02\ 10^{44}$	8.3	77
Pegas.	23 17 42.6	+07 55 57	3888	3519	393	$<6.3\ 10^{42}$	–	18
A2634	23 35 59.1	+26 45 14	9240	8895	661	$5.22\ 10^{43}$	3.4	60

[a] L_X measured in the 2–10 keV band.
[b] The fraction of HI deficient objects was computed considering NGC 383 and NGC 507 together.
[c] Group A of Bothun et al. (1983).

Coma

Coma is the prototype rich cluster in the local Universe, and one of the best studied, together with the Virgo cluster. At a radial heliocentric velocity of 6917 km s^{-1} (Zabludoff *et al.* 1990), Coma is located within a region of moderately high galaxy density, usually referred to as the Coma Supercluster, which is part of the so-called "Great Wall" (see for example de Lapparent *et al.* 1986). It is classified as of richness class 2 by Abell (1958), and is morphologically classified as a binary cluster (Sastry & Rood 1971), dominated by the 2 giant ellipticals NGC 4874 and NGC 4889. The X-ray morphology is that of a well evolved, dynamically relaxed cluster. In the cluster central region the galaxy population is composed approximately of 30% ellipticals, 56% S0's, and 14% spirals (Dressler 1980b), with strong morphological segregation. HI deficiency is very pronounced among the spiral galaxy population (the fraction of deficient objects is 77%; Giovanelli & Haynes 1985).

A2634

A2634 is a moderately rich cluster, that provides a good example of an intermediate cluster, between a rich cluster like Coma and rather poor clusters like A262 or Pegasus. At a radial heliocentric velocity of 9240 km s^{-1} (Scodeggio *et al.* 1995), A2634 is located in a region of complex topology, with a companion (A2666) only 3° to the East, and at least a foreground and a background group projected in its vicinity (see the discussion in section 2.3). It is classified as of richness class 1 by Abell (1958), and morphologically as a cD cluster (Sastry & Rood 1971), dominated by the giant elliptical NGC 7720. The X-ray morphology is that of a well evolved, dynamically relaxed cluster. In the cluster central region the galaxy population is composed approximately of 17% ellipticals, 46% S0's, 37% spirals (Dressler 1980b), with strong morphological segregation. HI deficiency is very pronounced among the spiral galaxy population (the fraction of deficient objects is 60%; Solanes 1996).

A1367

A1367 is an irregular, spiral rich cluster, quite different from the dynamically relaxed and regular Coma and A2634. At a radial heliocentric velocity of 6408 km s^{-1} (Zabludoff *et al.* 1990), A1367 is part of the Coma Supercluster and the "Great Wall". It is classified as of richness class 2 by Abell (1958), and is morphologically classified as an irregular cluster (Sastry & Rood 1971). The X-ray morphology is also irregular, typical of a rather young and not yet dynamically relaxed cluster. In the cluster central region the galaxy population is composed approximately of 17% ellipticals, 40% S0's, 43% spirals (Giovanelli & Haynes 1985), with a modest morphological segregation. HI deficiency is quite evident among the spiral galaxy population (the fraction of deficient objects is 42%; Giovanelli & Haynes 1985).

A262

A262 is a rather poor cluster that is the prototype of a particular class of objects brought into evidence by the first imaging X-ray astronomical observations. Specifically, these clusters have rather low X-ray luminosity and velocity dispersion, cool ICM temperature, and high spiral fraction, all indicative of dynamical youth, coexisting with the presence of a massive dominant galaxy, which is typical of a dynamically evolved cluster. At a radial heliocentric velocity of 4896 km s^{-1} (Zabludoff *et al.* 1990), A262 is part of the Perseus-Pisces Supercluster. It is classified as of richness class 0 by Abell (1958), and is morphologically classified as a regular, centrally condensed cluster (Sastry & Rood 1971), dominated by the giant elliptical NGC 708. In the cluster central region the galaxy population is composed approximately of 21% ellipticals, 32% S0's, 47% spirals (Giovanelli & Haynes 1985), with some morphological segregation. HI deficiency is quite evident among the spiral galaxy population (the fraction of deficient objects is 48%; Giovanelli & Haynes 1985).

Pegasus

Pegasus is a poor, rather irregular, spiral rich cluster. At a radial velocity of 3888 km s^{-1}, it is too close to be included in the Abell (1958) catalogue. The center of the cluster is dominated by the giant elliptical NGC 7621, and the galaxy population is composed approximately of 12% ellipticals, 29% S0's, 59% spirals (Giovanelli & Haynes 1985), with little morphological segregation. The only detected X-ray emission is considered to be associated with the central elliptical, and any diffused ICM present in this group must have quite a low density. As a result, only a modest amount of HI deficiency is present among the spiral galaxy population (the fraction of deficient objects is 18%; Giovanelli & Haynes 1985).

Cancer

What has been traditionally identified as the Cancer cluster is in fact a superposition of many different rich groups, perspectively projected over a rather small area in the sky (Bothun *et al.* 1983). Here we consider as a cluster only the largest of those groups (group A in Bothun *et al.* classification), at a radial heliocentric velocity of 4705 km s^{-1}. This is a spiral-rich group, composed of 11% ellipticals, 18% S0's, 71% spirals (Giovanelli & Haynes 1985). X-ray emission has been detected, but it is generally considered to be associated with the brightest galaxy in the group, the elliptical NGC 2563. If any truly diffused ICM is present in this group, it must have quite a low density. This is also made evident by the modest presence of HI deficiency among the spiral galaxy population (the fraction of deficient objects is 21%; Giovanelli & Haynes 1985).

NGC 507 and NGC 383 groups
The NGC 507 and NGC 383 groups are often considered together as a single object, the so-called Pisces cluster. However they were clearly identified as two separate units by Sakai *et al.* (1994), although with very similar redshift. The two groups are then identified with the name of the respective brightest member. Both are embedded into the Perseus-Pisces Supercluster, at radial heliocentric velocities of 5091 and 5161 km s^{-1} (Sakai *et al.* 1994), respectively. In both cases the galaxy population is dominated by elliptical and S0 galaxies. As in the case of Cancer, X-ray emission is considered to be associated with the brightest groups members, and any ICM eventually present must have a rather low density. Also, HI deficiency is almost completely absent among the spiral galaxy population (the fraction of deficient objects is 10%; Solanes 1996). The separation line between the two groups is necessarily somewhat arbitrary, but the percolation analysis performed by Sakai *et al.* (1994) shows that there is no ambiguity in the membership assignment of the early-type galaxies in the central region of both groups.

2.2 Cluster membership

For all clusters and groups at distances greater than 10–15 Mpc, membership assignment is done solely on the basis of redshift information, using Hubble's law to transform redshifts into distances. However, because of virial motions within the cluster potential well, cluster members display a distribution of radial velocities, centered on the mean recessional velocity of the cluster. Of course it is practically impossible to separate cluster members with a large component of their virial velocity directed along the line of sight from foreground or background objects that have the same radial velocity. Therefore the determination of the true shape of a cluster velocity distribution is a circular problem, that is often solved using an iterative scheme. After a first estimate of the distribution has been obtained, using all galaxies projected within a given distance from the cluster center, a sigma-clipping procedure is used to eliminate the most likely foreground and background objects. Then a new estimate of the distribution is obtained, and the procedure repeated until no more rejections occur. At this point, all objects that were not rejected by the clipping procedure are considered to be cluster members (see for example Yahil & Vidal 1977).

Whenever a large number of redshift measurements is available, it is possible to obtain more reliable membership assignments using the information contained not only in the velocity distribution of the cluster members, but also in their spatial distribution (Kaiser 1987). In a very naïve rendition, the method works as follows. Redshifts measure only the radial component of a galaxy velocity, and therefore projection effects alter our ability to measure the true virial velocity of a galaxy within a cluster. Because the true velocity distribution of cluster members is bound by the cluster escape velocity, the maximum range of cluster members' radial velocities that can be observed decreases with increasing angular distance from the cluster center. Thus there should exists a sharp boundary, in angular separation - radial velocity space, between bounded and unbounded objects (i.e. between cluster and field galaxies). The lines that mark this boundary are generally referred to as redshift space caustic curves. Detailed derivations of this caustic lines method have been presented by Regös & Geller (1989), and by van Haarlem (1992). A detailed example of its application is presented in section 2.3.3, for the cluster A2634. Unfortunately, the computation of the caustic lines relies on a large number of simplifying assumptions, and on the value of cosmological parameters like $\Omega_\circ$, and when applied to real clusters not even this method provides completely unambiguous determinations of cluster membership.

Coma

The first detailed dynamical analysis of the Coma cluster was presented by Kent & Gunn (1982). Redshift space caustic lines for Coma have been published by Regös & Geller (1989), van Haarlem (1992), and Gavazzi, Randone & Branchini (1995). The cluster is well separated in redshift space from both the foreground and the background field, and membership can be reliably assigned to objects to an angular separation of approximately 5 degrees from the cluster center. Following the criterion used by G97a, we define as cluster members all galaxies within 4 degrees from the cluster center that fall within the radial velocity limits defined by the Regös & Geller (1989) caustic curves estimated for $\Omega_\circ = 0.3$. The center of the cluster, following Kent & Gunn (1982), is assumed to be at the position of the brightest galaxy NGC 4874: $12^h57^m11^s.1$ +28°13'48". The substructure within the Coma cluster recently discussed by Colless & Dunn (1996) appears to be insignificant for our discussion. The difference in radial distance between the merging sub-units is only a small fraction of the distance to the Coma cluster, and might cause just a small enhancement in the dispersion observed in the TF and FP diagrams.

A2634

The first in–depth redshift survey of A2634 was carried out by Pinkney *et al.* (1993). A more detailed study of the cluster structure was carried out by Scodeggio *et al.* (1995; hereafter S95), who also estimated redshift space caustic lines. A2634 is located in a region of higher complexity than that containing Coma. The cluster A2666 ($cz_{hel} = 8134$ km s^{-1}) lies 3° to the East of A2634 ($cz_{hel} = 9240$ km s^{-1}); two more groups, one in the foreground ($cz_{hel} = 7546$ km s^{-1}) and one in the background ($cz_{hel} = 11{,}619$ km s^{-1}), were identified by S95, projected respectively 1.1 and 0.6 degrees to the NE and to the SE of A2634. In addition, two background clusters, A2622 at $cz_{hel} = 18{,}345$ km s^{-1}, and an anonymous cluster at $cz_{hel} = 37{,}093$ km s^{-1}, are projected to within less than 1 degree from the center of A2634. We define as A2634 members all galaxies within 2.5 degrees from the cluster center that fall within the radial velocity limits defined by the S95 caustic curves corresponding to $\Omega_\circ = 0.3$. The cluster center is assumed to be at the position of the cD galaxy NGC 7720: $23^h35^m59^s.1$ +26°45'14". A more detailed study of A2634 is presented in the next section.

A1367

Redshift space caustic lines for A1367 have been published by Regös & Geller (1989), and Gavazzi, Randone & Branchini (1995). A1367 is part of the Coma Supercluster, and, as in the case of Coma, the cluster is fairly well separated in redshift space from foreground and background objects. Following the criterion used by G97a, we define as cluster members all galaxies within 3 degrees from the cluster center that fall within the radial velocity limits defined by the Regös & Geller (1989) caustic curves estimated for $\Omega_\circ = 0.3$. The center of the cluster is assumed to be at the mid-point between the two brightest elliptical galaxies in the cluster, NGC 3842 and NGC 3862: $11^h41^m57^s.0$ $+20^\circ03'30''$. This is also very close to the centroid of the X-ray emission.

A262

Sakai *et al.* (1994) presented a detailed analysis of the spatial and velocity distribution of the galaxies in the A262 area. Although they did not derive redshift space caustic lines for this cluster, their work can be used to derive reliable membership criteria, out to a radial distance of 1.5 degrees from the cluster center. At larger distances, the contamination from the sparse population of the Perseus-Pisces Supercluster becomes quite significant. We define as A262 members all galaxies within 2 degrees from the cluster center, with radial heliocentric velocity within the interval 3500–6300 km s^{-1}. The center of the cluster is assumed to be at the position of the dominant galaxy NGC 708: $1^h49^m49^s.9$ $+35^\circ54'21''$.

Pegasus

No redshift space caustic lines are available for Pegasus. The cluster, however, is quite well separated in redshift space from foreground and background objects, and membership assignments are not problematic, at least for the early-type population. We define as Pegasus members all galaxies within 2 degrees from the cluster center, with radial heliocentric velocity within the interval 2700–5100 km s^{-1}. The center of the cluster is assumed to be at the position of the dominant galaxy NGC 7621: $23^h17^m42^s.6$ $+07^\circ55'57''$.

Cancer

Bothun *et al.* (1983) have provided the first identification of the different groups into which the so-called Cancer cluster can be divided. Their analysis shows quite clearly the combined spatial and velocity segregation of the different groups. Here we consider as Cancer cluster the largest of those groups (group A in Bothun *et al.* 1983), centered on the elliptical galaxy NGC 2563, and follow Bothun *et al.* membership assignments to select members of this group. The center of the cluster is assumed to be at the position of the dominant galaxy NGC 2563: $8^h17^m40^s.7$ $+21^\circ13'36''$.

NGC 507 and NGC 383 groups

Sakai *et al.* (1994) presented a detailed analysis of the spatial and velocity distribution of the galaxies in the NGC 507 and NGC 383 groups area. The available redshift samples are too small to derive redshift space caustic lines for these groups, but membership can be assigned quite confidently nonetheless, thanks to the relative underdensity of the region in front and behind the Supercluster the two groups are part of. Here we ignore the possible separation of the NGC 529 and NGC 410 groups as separate entities (see Sakai *et al.* figure 5), because these small compact groups (4 and 5 members) are at the same redshift as the two main ones. Therefore we define as NGC 507 members all galaxies within 1.5 degrees from the group center, with radial heliocentric velocity within the interval 3500–6700 km s^{-1}, and as NGC 383 members all galaxies within 1.0 degrees from the group center, with radial velocity within the interval 3800–6500 km s^{-1}. The centers of the two groups are assumed to be at the positions of the two dominant galaxies: NGC 507 at $1^h20^m51^s.1$ $+32^\circ59'40''$, and NGC 383 at $1^h04^m39^s.4$ $+32^\circ08'46''$.

2.3 A2634: a case study[1]

The development of multifiber spectroscopy has made possible the simultaneous acquisition of tens of galaxy spectra. As a result, the study of the dynamics of clusters of galaxies is enjoying the availability of extensive and more complete new redshift data bases, which reveal the complexity of detail in cluster structure and help to solve the problems plaguing the interpretation of the kinematical data like projection effects, velocity anisotropy, substructure and secondary infall. Here, we present the results of an extensive observational effort to expand the kinematical data base for A2634, and a detailed analysis of the structure and dynamics of that cluster.

A $12^o \times 12^o$ field centered on A2634 was visually surveyed on the Palomar Observatory Sky Survey (POSS) blue prints, identifying galaxies with major diameter larger than about 0.5arcmin. Coordinates for these objects were measured with few arcsec accuracy using a measuring machine developed by T. Herter. This search was carried out to obtain a list of candidates for future TF work. In addition, the inner square degree of this region was searched using the FOCAS software package, on digitized images of the Palomar Quick Survey, obtained with the kind assistance of D. Golombek of the Space Telescope Science Institute. This search produced a list of galaxy positions and rough indicative magnitudes which is estimated to be complete to a limiting magnitude near 16.5, although numerous fainter galaxies are included. About half of the galaxies in the first spiral sample were observed with the Arecibo 305m radio telescope in the 21 cm line. An effort was made to include all the galaxies in the inner region brighter than 16th magnitude among those targeted by an optical spectroscopic survey carried out with the 5m Hale telescope of the Palomar Observatory. Because the spectra were in great part obtained with a multifiber spectrograph, many targets were included for reasons of observational expedience rather than responding to strict flux or size criteria. As a result, the limits of our spectroscopic survey are blurred, and can roughly be represented by a completeness function which, in the inner square degree is 1 at $m_{pg} \sim 15.7$, 0.85 near 16.0, and drops below 0.5 at magnitudes fainter than 16.5.

2.3.1 New Redshifts

New redshifts of 174 galaxies in the $12^o \times 12^o$ field centered on A2634, which also includes A2666, were measured. Redshifts for 37 additional galaxies located within that same region were obtained for a separate but complementary study (Giovanelli *et al.* 1994).

The red camera of the double spectrograph (Oke & Gunn 1982) was used on September 25, 1992 to obtain single slit spectroscopy for 41 galaxies in our catalog. A grating with 316 lines mm^{-1} was used to produce spectra in the range 4900–7300 Å, with a typical resolution of 9.6 Å. The detector was a TI 800×800 CCD chip. The data were reduced following standard procedures with available IRAF[2] tasks. Each frame was overscan- and bias-subtracted, then flat-fielded using appropriate dome flats. Wave-

[1]This section is based on the paper: Scodeggio, M., Solanes, J.M., Giovanelli, R., & Haynes, M.P. 1995, "The Spatial Distribution, Kinematics, and Dynamics of the Galaxies in the Region of Abell 2634 and 2666", ApJ 444, 41 [copyright 1995 by The American Astronomical Society].

[2]IRAF (Image Reduction and Analysis Facility) is distributed by the National Optical Astronomy Observatories, which are operated by the Association of Universities for Research in Astronomy, Inc., under contract with the National Science Foundation.

length calibration was performed using He-Ne-Ar lamp comparison spectra before and after each source observation. Heliocentric velocities were computed in two different ways: using the IRAF task *fxcor*, which is based on the cross-correlation algorithm described by Tonry & Davis (1979), for pure absorption spectra, and measuring the central wavelength of the Gaussian fit to the emission lines of spiral galaxies (typically between 3 and 7 lines were measured for each galaxy). Three different K giant stars were used as templates for the cross-correlation.

The Norris multifiber spectrograph (Hamilton et al. 1993) was used on October 20, 1993 to observe a fainter sample of galaxies in the central region of A2634 and A2666. The Norris spectrograph has a field of view of 20 arcmin, within which 176 independent fibers can be placed for photon acquisition. At the front end, the fibers subtend 1.6 arcsec, and can be placed as close as 16 arcsec apart. The fiber outputs are transferred through a grating element to a CCD detector. At the time of these observations, the Tektronik CCD had a reduced format of 1024×1024, restricting the number of usable fibers to half the total and the field of view to a 10arcmin$\times$20arcmin region. Coordinates for the target galaxies were measured on the digitized Palomar "quick V" survey plates at STScI. A 300 lines mm^{-1} grating was used to produce spectra in the range 4500–7000 Å, with a resolution of 7.5 Å. Each frame was first overscan- and bias-subtracted, then one-dimensional spectra were extracted using appropriately sized apertures. These spectra were wavelength-calibrated using He-Ne-Ar comparison lamp spectra taken with the fibers deployed as for the galaxy acquisition, and extracted using the same apertures used for the object spectra. The sky subtraction was performed subtracting from each one of the object spectra the median of the output of ten fibers positioned on blank sky positions, properly scaled in order to compensate for light transmission variations from fiber to fiber. After the final one-dimensional spectra were obtained, velocities were derived with precisely the same procedure described above for the single slit spectra. Two different K giant stars were used as templates for the cross-correlation.

New 21 cm observations of 89 galaxies in the A2634/2666 region were carried out between 1990 and January 1994. In all cases the observational setup was as described in Giovanelli & Haynes (1989). Since this sample includes galaxies significantly fainter than those customarily observed in 21 cm emission, integration times averaged 0.7 hours per object on source. Typical rms noise per averaged spectrum ranged between 0.3 and 0.9 mJy. The later set of observations (July 1993 to January 1994, approximately 25% of all runs) benefited from the completion of Phase I of the Arecibo telescope ongoing upgrading project (Hagfors et al. 1989), which includes the construction of a ground screen, 15 meters high and covering an area of 14,700 m^2 around the main dish. The principal benefit of this device is a drastic reduction in the amount of ground radiation pickup, allowing a significant reduction of system temperature and an increase in the telescope sensitivity for observations with zenith angles higher than 10 deg. All observations were taken with a spectral resolution of approximately 8 km s^{-1}, later reduced by smoothing by an amount dependent on the signal-to-noise ratio.

The results of those observations were published in S95 (Tables 1, 2, and 3), and are not presented here again.

2.3.2 The Environment of A2634

The cluster A2634 appears projected on the main ridge of the Pisces-Perseus Supercluster (hereinafter referred to as PPS; see Figure 1 of Wegner, Haynes, & Giovanelli 1993), although it and its close companion A2666 are actually located on the higher redshift branch of the two into which the PPS splits near R.A. = 00^h45^m. Figure 2.1 displays the positions of 663 galaxies with known redshift in the $12^o \times 12^o$ region centered on A2634. Of those, 237 are redshifts obtained from our previous surveys (Giovanelli & Haynes 1985, 1989, 1993; Giovanelli et al. 1986b; Wegner et al. 1993), 215 are listed in Pinkney *et al.* (1993) and 211 are the new determinations presented in S95 and in Giovanelli et al. (1994). In Figure 2.1, filled circles are used for objects with $m_{pg} \leq 15.7$ for which the redshift survey is virtually complete in the whole field, while open circles are used for galaxies fainter than that limit. Note that the latter are clearly more concentrated towards the cluster inner regions due to the observational bias towards the core of A2634 produced by the multifiber spectrograph observations. In Figure 2.2 a radial velocity histogram between 0 and 45,000 km s^{-1} of the galaxies in Figure 2.1 is shown: the significant peak near 5500 km s^{-1} is associated with the foreground branch of the PPS; the peak near 8000 km s^{-1} includes principally galaxies in the redshift domain of A2666; the highest peak near 9000 km s^{-1} is associated with A2634; and a well defined group around 11,700 km s^{-1} appears detached from the A2634 regime. The feature around 18,000 km s^{-1} includes the rich Abell cluster A2622 (centered 0.9^o to the NW of A2634) and several more widely spread galaxies. The velocity peak near 37,000 km s^{-1} is produced by a noticeable concentration of galaxies almost directly behind the A2634 center. Pinkney *et al.* (1993) tentatively associate the X-ray clump seen in the *Einstein* IPC map of A2634 to the northwest of A2634 itself (see their Figure 4) with this background distant cluster.

2.3.3 Cluster membership

As a first quantitative step in our analysis, we have assigned cluster/group membership to the galaxies in our $12^o \times 12^o$ sample. Usually, cluster membership is assigned using only a fixed range of velocities. The velocity distribution of all galaxies projected within a chosen distance from the cluster center is obtained and field galaxy contamination is eliminated, typically via a 3σ-clipping technique (Yahil & Vidal 1977) or using procedures that take into account the gaps of the observed velocity distribution. At this point, all galaxies within two fixed velocity limits are assigned to the cluster. These methods do not consider the fact that, with the exception of the virialized inner cluster regions where a roughly constant velocity dispersion is expected, the line-of-sight velocity dispersion of true cluster members decreases with increasing projected separation from the cluster center, whether the cluster is bound and isolated or whether a significant amount of secondary infall is present. This consideration will be taken into account in the subsequent membership assignment for the best sampled cluster A2634.

Because of the proximity between A2634 and A2666, we first proceed to identify those galaxies in the neighborhood of A2634 that are more likely to be associated with A2666. To accomplish that, we compare the projected number density profiles of the two clusters at the position of any given galaxy, and assign it to A2666 if this cluster's density profile has a higher value than that of A2634 at that location. The projected number density

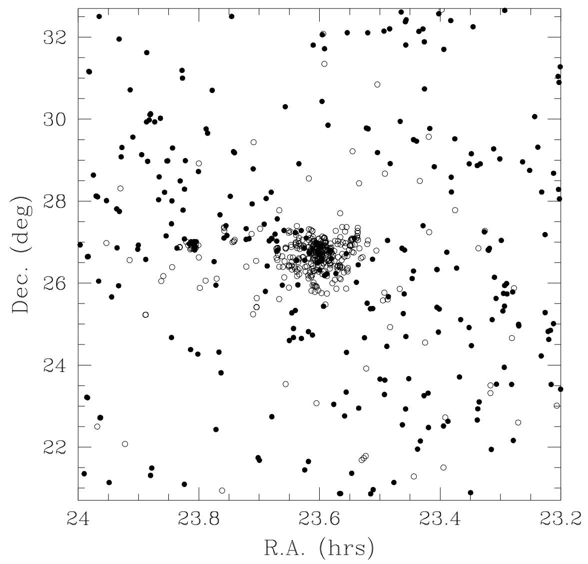

Figure 2.1 Spatial distribution of galaxies with known redshift in the 12°×12° field around A2634's center. Galaxies with $m_{pg} \leq 15.7$ are identified with filled circles, while open circles are used for those fainter than that limit.

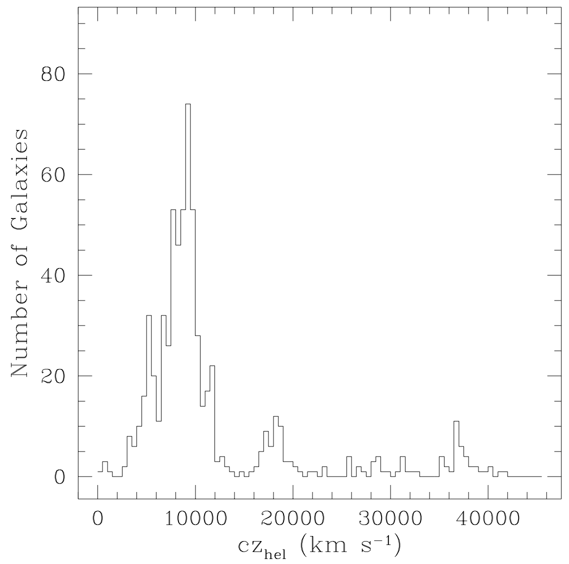

Figure 2.2 Radial velocity histogram up to 45,000 km s^{-1} for the galaxies in the 12°×12° field around A2634's center . Bins are 500 km s^{-1} in width.

profile of A2634 has been determined applying the so-called "direct method" of Salvador-Solé, Sanromá, & González-Casado (1993a) to the Dressler's (1980b) magnitude-limited sample of A2634 galaxies, which covers the inner region of the cluster up to a radial distance of $\sim 0.5^{\circ}$ from its center (within this region a negligible contamination by galaxies belonging to A2666 is expected as the two clusters are separated by 3°). A good fit to the numerical solution given by this method is obtained using a modified Hubble-law of the form

$$N(X) = N(0)[1 + X^2]^{-\gamma+1/2} , \tag{2.1}$$

where $N(0)$ is the central projected number density of galaxies, γ a shape index, and $X = s/r_*$ the projected distance s to the center of the cluster in core radius units r_*. The best fitting values of the parameters $N(0)$, γ and r_* for A2634 are: 69 galaxies Mpc^{-2}, 1.5, and 0.48 Mpc, respectively. For A2666, the scarcity of observations makes the above procedure more uncertain; we then assume, for simplicity, that the values of the shape index and core radius of both clusters are the same and that they have the same mass-to-light ratio. Next, for each galaxy in the sample with heliocentric velocity in the range 6500–9500 km s^{-1} (which we adopt as the velocity boundaries of A2666; see S95, we compute the projected distances to A2624, X_{34}, and A2666, X_{66}, and assign A2666 membership if $N(X_{66}) > N(X_{34})$ or, equivalently, if

$$X_{66} < \left[\frac{M_{66}}{M_{34}}(1 + X_{34}^2) - 1\right]^{1/2} , \tag{2.2}$$

where M_{66}/M_{34} is the ratio of the masses of the two clusters, which we take equal to 1/7 (see S95 and section 2.3.6). It is worthwhile to mention that the exact values adopted for the ratio of cluster masses (or, equivalently, the ratio of central projected number densities), γ and r_*, have a negligible practical influence on the results to be discussed later on, so any further refinement of this procedure is unnecessary.

In Figure 2.3 we plot the heliocentric velocity as a function of the angular separation θ for all galaxies within 6° of the A2634's center. Unfilled symbols identify probable A2666 members using the procedure described above. Since contamination from A2666 starts to be present at $\theta > 2^{\circ}$, we choose to restrict our following analysis to galaxies within this distance from the center of A2634. The solid lines plotted in Figure 2.3 are the caustics associated with A2634 derived using the spherical infall model described in Regös & Geller (1989). In this simple model, the amplitude of the caustics depends only on $\Delta(r)$, the mass overdensity profile of the cluster, and the cosmological density parameter Ω_0. To determine the former, we have followed the procedure outlined by Regös & Geller (1989), which relies on the assumption that the galaxies trace the mass distribution, i.e., that $\Delta(r)$ is identical to the *number* density enhancement of galaxies in the cluster:

$$\Delta(r) = \frac{<\rho>}{\rho_u} - 1 = \frac{<n>}{n_u} - 1 . \tag{2.3}$$

In equation (2.3), $<\rho>$ and $<n>$ are, respectively, the average mass and number density of cluster galaxies (corrected for field contamination) inside a radius r, whereas ρ_u and n_u are the mean mass density and the mean number density of galaxies in the universe. The spatial distribution of galaxies $n(r)$ has been estimated by inverting the analytical fit to the observed projected number density profile $N(r)$ given by eq. (2.1). The mean number density of field galaxies n_u has been calculated by integrating the Schechter (1976) luminosity function obtained from the CfA survey (de

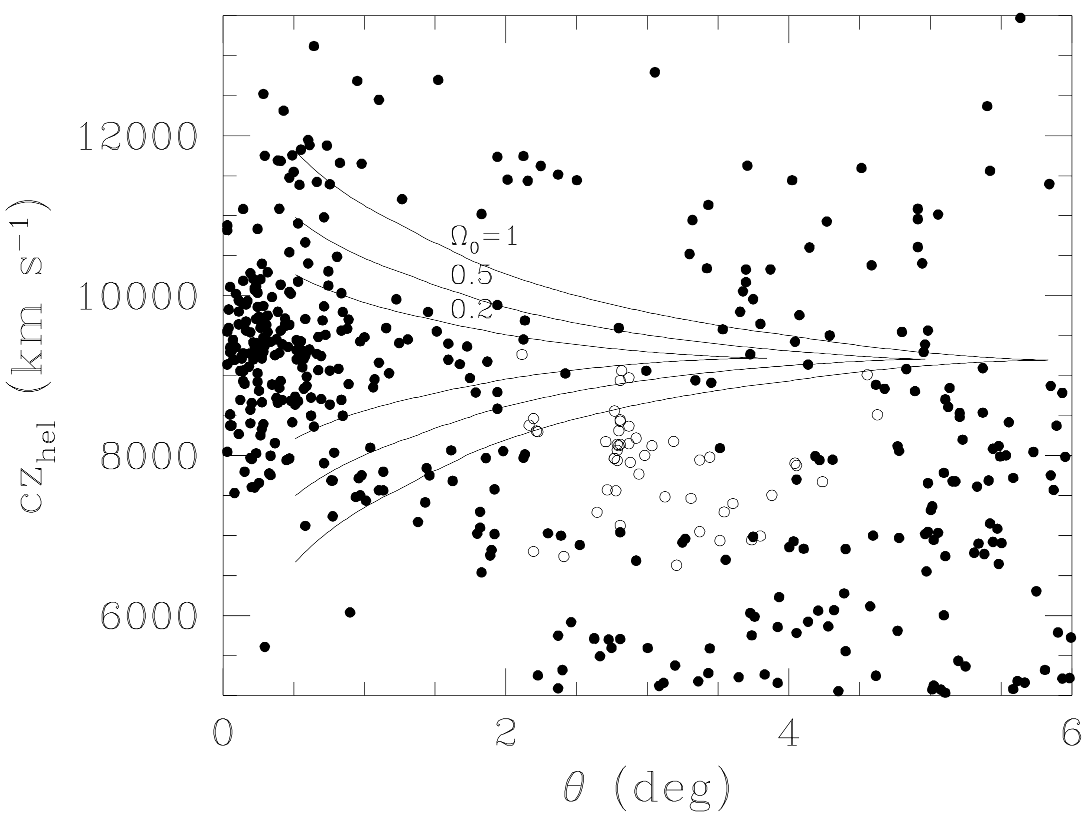

Figure 2.3 Heliocentric velocity vs. angular separation for all galaxies within 6°from the center of A2634. Unfilled symbols identify probable A2666 members in the range $6500 \leq V_{hel} \leq 9500$ km s^{-1}. Solid lines are the predicted caustics for three different values of Ω_0.

Lapparent, Geller, & Huchra 1989) to the limiting magnitude of the Dressler sample, $m_v = 16.0$. This has been converted to the $B(0)$ scale of the CfA survey assuming $m_{B(0)} - m_v = 0.8$. We obtain $n_u = 2.28 \times 10^{-3}$ galaxies Mpc^{-3}.

The caustics of Figure 2.3 correspond to $\Omega_0 = 0.2, 0.5$, and 1, the amplitude increasing with the value of Ω_0. Clearly, no sharp boundary is observed in the velocity distribution of the galaxies in this sample that would mark the transition between the triple-valued and single-valued regions, which suggests that some of the simplifying assumptions implicit in the Regös & Geller model are probably too stringent (see, for instance, van Haarlem et al. 1993). But the caustics derived from the spherical infall model can still be used effectively to accomplish our purpose of defining strict cluster membership if they are supplemented by further inspection of both the spatial and velocity distribution of candidate A2634 members. Figure 2.4a shows an enlargement of Figure2.3 , focusing on galaxies in the inner 2° around the center of A2634, while Figure 2.4b displays their corresponding sky distribution. Two groups of galaxies between the $\Omega_0 = 0.5$ and $\Omega_0 = 1.0$ caustics can be separated from strict cluster members: one group probably located in the foreground of the cluster between 7000 and 8000 km s^{-1}, and a second in the background between 11,000 and 12,000 km s^{-1} already identified as a detached group by Pinkney *et al.* (1993). Both groups have small velocity dispersions, are separated by large gaps in radial velocity from other galaxies at a comparable distance from the cluster center and appear to be concentrated in small areas in the sky, to the east of the A2634 core (approximately 1.5° to the southwest of the center of A2634 there is a possible third group of foreground objects with velocities around 7000 km s^{-1}, but the evidence for its physical reality is poor). We assign separate dynamical identity to these two groups. Accordingly, we chose to consider *bona fide* A2634 members only those galaxies inside the $\Omega_0 = 0.5$ caustic. We caution again that this choice represents more an operational criterion for defining cluster membership than a statement on the value of Ω_0.

2.3.4 Kinematics and Spatial Analysis of A2634

Following the recommendations of Beers, Flynn, & Gebhardt (1990), we characterize the velocity distribution of the A2634 galaxies by means of the biweight estimators of central location, V (i.e., systemic velocity, sometimes in the literature referred to as C_{BI}), and scale, σ (i.e., velocity dispersion, sometimes in the literature referred to as S_{BI}), because of their robustness (i.e., insensitivity to the probabilistic model adopted for the observed data) and resistance (i.e., insensitivity to the presence of outliers). The errors associated with these estimates, ϵ_V and ϵ_σ respectively, correspond to 68% bootstrap confidence intervals based on 10,000 resamplings. The program ROSTAT, kindly provided by T. Beers, is used for all these calculations. Among the wide variety of statistical tests implemented in this program to assess the gaussianity of the empirical distribution, we quote here the results for the W-, B_1-, B_2-, and A^2-tests (definitions of these tests can be found, for instance, in Yahil & Vidal 1977 and D'Agostino 1986). The scaled tail index TI (Rosenberger & Gasko 1983; see also Bird & Beers 1993) is applied to determine the amount of elongation of the empirical distribution relative to the Gaussian (which is neutrally elongated by definition: TI=1.0). Distributions which have more strongly populated tails than the Gaussian have TI>1.0, while those with underpopulated tails have TI<1.0. Finally, we also investigate the existence in the velocity distribution of

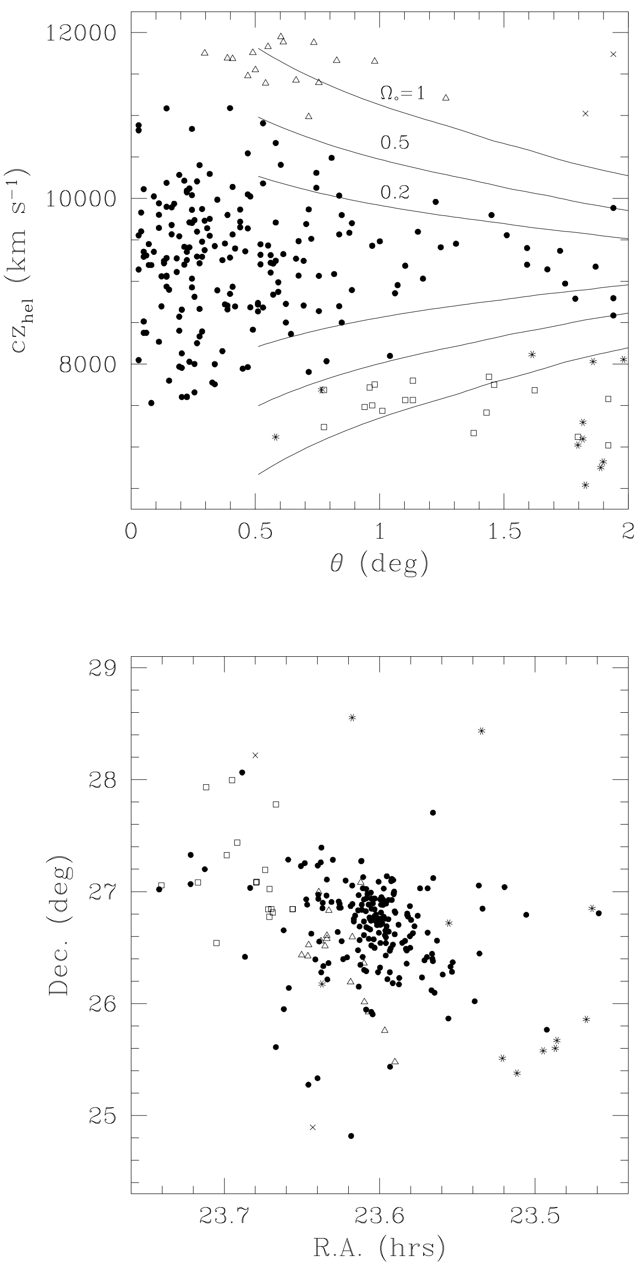

Figure 2.4 (a) Heliocentric velocity vs. angular separation for the galaxies in the inner 2° around the center of A2634. Solid lines are the predicted caustics for three different values of Ω_0. (b) Corresponding spatial distribution. In both figures large open squares identify the 18 galaxies associated with a foreground group, while large open triangles identify the 17 members of a background group. Large asterisks and crosses mark, respectively, foreground and background galaxies outside the caustic $\Omega_0 = 0.5$ and not belonging to any of these two groups. Filled circles identify bona fide members of A2634.

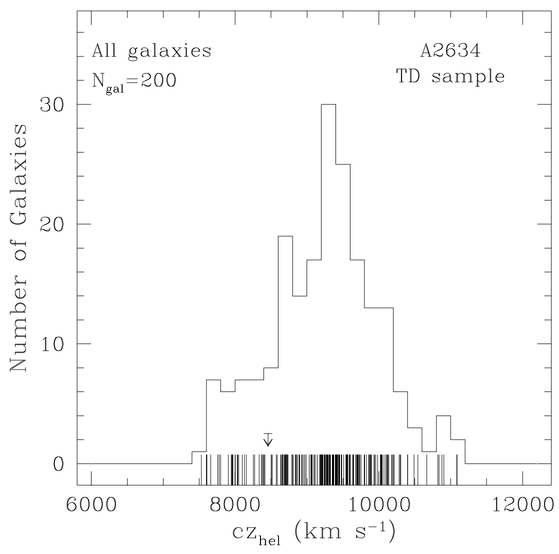

Figure 2.5 Stripe density plot and velocity histogram for all the galaxies in the A2634 TD sample. Arrows mark the location of the most significant weighted gaps in the velocity distribution (see text).

weighted gaps of size 2.75 or larger, corresponding to a probability of occurrence in a normal distribution of less than 1% (Beers et al. 1990). We refer the reader to the listed references for a detailed explanation of these statistical techniques.

If the statistical sample is large enough, the analysis of the possible correlation between galaxy morphology and kinematics provides a tool that is helpful in assessing the dynamical and evolutionary state of a cluster of galaxies. Several studies (e.g., Kent & Gunn 1982; Tully & Shaya 1984; Sodré, Capelato, & Steiner 1989) show evidence for a higher velocity dispersion of the spiral population than that of the early-types in clusters. This result is consistent with the idea that the spiral galaxies are currently infalling and have not suffered appreciable dynamical mixing with the virialized core. Should this picture turn out to be correct, it would imply that either the spiral fraction in clusters is increasing with time, and/or that environmental effects are an important factor in determining galaxy evolution and the relation between morphology and density, transforming spiral galaxies into earlier morphological types. For this reason, we split each one of the samples selected for A2634 into two subsets of early- and late-type galaxies and comparatively investigate their kinematics and spatial distribution.

After the contamination due to nearby groups has been removed via the procedure described in the previous section, our sample of bona fide A2634 members within a radius of 2 degrees (hereinafter referred to as the "TD sample") is composed of 200 galaxies. The stripe density plot of heliocentric radial velocities and the corresponding histogram for this sample are shown in Figure 2.5. For this sample $V_{hel} = 9249^{+55}_{-56}$ km s^{-1} and $\sigma = 716^{+48}_{-35}$ km s^{-1} after applying relativistic and measurement error corrections (Danese, De Zotti, & di Tullio 1980). The visual inspection of Figure 2.5 yields suggestive but inconclusive indication of deviation of the velocity distribution from gaussianity. The dictum of statistical tests, unsurprisingly, is equally ambiguous. The results of the B_1-, B_2- and A^2-tests do not indicate significant departures from normality. However, the W-test gives only a 7% probability that the observed distribution could have arisen by chance from a parent Gaussian population. The tail index TI indicates slight contamination of the tails of the distribution with respect to the Gaussian. The velocity distribution also contains one highly significant weighted gap, indicated by the arrow in Figure 2.5. The size of the corresponding gap is 83 km s^{-1}. The presence of this gap in the observed distribution suggests, —but only weakly—, that the underlying parent distribution may be kinematically complex.

For the TD sample, its subdivision into two subsets of early- (E and S0) and late-type (S and Irr) galaxies reveals that the kinematical characteristics of the two populations are different. Figure 2.6a shows the stripe density plot of radial velocities and histogram for the early-type subsample, which has $V_{hel} = 9276^{+67}_{-73}$ km s^{-1} and $\sigma = 658^{+62}_{-42}$ km s^{-1}. Despite the low value of the tail index (TI=0.91) and the existence of one highly significant gap of size 94 km s^{-1} (identified with the arrow in Figure 2.6a) near 9000 km s^{-1} that weakly suggest possible bimodality in the parent distribution, none of the gaussianity tests reveals inconsistency with a normal parent population. On the contrary, the velocity distribution of the late-type subsample represented in Figure 2.6b is clearly non-Gaussian (the most sensitive tests of normality, W and A^2, reject the Gaussian hypothesis at better than the 3% level of significance) and bimodal. Two highly significant and very close gaps of 334 and 192 km s^{-1}, can be seen at both sides of two galaxies with radial velocities of 8500 km s^{-1}, splitting the distribution of velocities into two modes which peak around 7700 and 9300 km s^{-1} and are responsible of the high value of the tail index (TI=1.23). The 7700 km s^{-1} mode contains four times fewer galaxies than the 9300 km s^{-1} mode, for which location and scale are approximately coincident with those of the velocity distribution of the early-type galaxies. This result implies that the low-velocity tail seen in the velocity histogram of the TD sample (Figure 2.5) is largely dominated by late-type galaxies (notice that the 10 likely nonmembers discussed in the Pinkney *et al.* 1993 study have already been removed from the present sample, as they all belong to the foreground and background groups discussed in the previous section). Although a two-sample Kolmogorov-Smirnov (KS) test gives a probability of 25% for the null hypothesis that early- and late-type subsamples are drawn from the same parent kinematical population, the systemic velocity of the late-type galaxies $V_{hel} = 9092^{+99}_{-126}$ km s^{-1} is marginally inconsistent, within the adopted uncertainties, with that of the early-type subsample.

Within the inner 0.5° from the center of A2634 it is possible to define a magnitude-limited sample with almost complete redshift coverage. This is composed by the 99 galaxies among those cataloged by Dressler (1980b) that are to be considered bona-fide A2634 members. We shall refer to this sample as the "HD sample". Figure 2.7 contains the stripe density plot and velocity histogram for the 99 galaxies in the HD sample. For this sample $V_{hel} = 9151^{+84}_{-91}$ km s^{-1} and $\sigma = 800^{+61}_{-52}$ km s^{-1}. The results of the W- and A^2-tests indicate a more significant departure from the Gaussian model than for the TD sample, giving probabilities of a Gaussian parent population of only 2% and 3%, respectively. The velocity distribution appears also relatively skewed, but the B_1-test cannot reject the Gaussian hypothesis ($p(B_1) = 0.29$). Similarly, the apparent bimodality of the velocity histogram is not supported by the presence of significant gaps in the velocity distribution. Figures 2.8 and 2.9 show, respectively, the velocity and spatial distributions of the subsets of early- and late-type galaxies. Although the

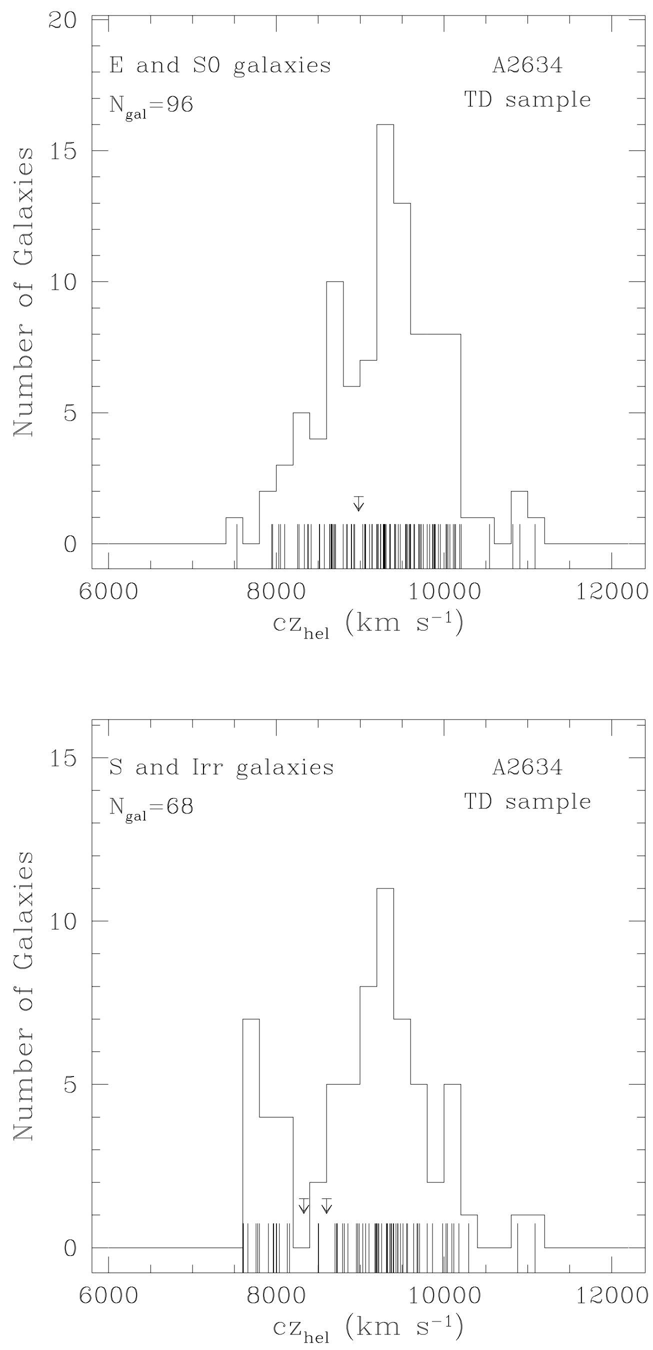

Figure 2.6 Stripe density plot and velocity histogram for (a) early-type galaxies, and (b) late-type galaxies in the A2634 TD sample. Arrows mark the location of the most significant weighted gaps in the velocity distribution.

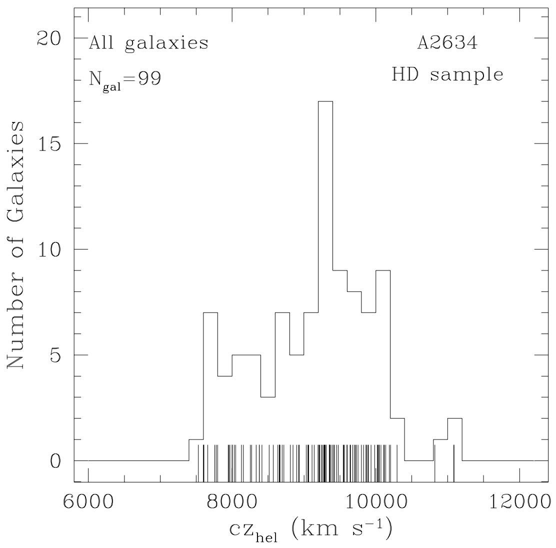

Figure 2.7 Stripe density plot and velocity histogram for all the galaxies in the A2634 HD sample. Arrows mark the location of the most significant weighted gaps in the velocity distribution.

velocity distribution of the E+S0 population has underpopulated tails (TI=0.89) and contains one highly significant gap of 146 km s^{-1} centered around 8770 km s^{-1}, all the statistical tests give markedly non-significant rejection levels for the Gaussian hypothesis. For this subsample $V_{hel} = 9240^{+79}_{-89}$ km s^{-1} and $\sigma = 661^{+74}_{-52}$ km s^{-1}. In contrast, the velocity distribution of the late-type subsample is clearly non-Gaussian, —with the exception of the B_1-test, the other tests reject the Gaussian hypothesis at better than the 3% significance level—, and multimodal, with suggestive evidence of three possible kinematical subunits with similar number of members. The small number of galaxies, however, hampers the detection of highly significant gaps: only one gap of 548 km s^{-1} centered around 8400 km s^{-1} falls within this category. Two of the modes are located in the lower and upper tails of the global velocity distribution, implying that only $\sim 1/3$ of the late-type galaxies have velocities close to the systemic velocity of the cluster. Accordingly, the main moments of the velocity distribution of this late-type subset, $V_{hel} = 8897^{+206}_{-246}$ km s^{-1} and $\sigma = 1030^{+116}_{-86}$ km s^{-1} have values that are incompatible, within the adopted uncertainties, with those of the early-type population.

Apart from the dynamical complexity of A2634, the HD sample also reconfirms the presence of significant morphological segregation in this cluster. Figures 2.8b and 2.9b show that the early-type galaxies dominate in the densest regions where the late-type galaxies are almost absent. Superposed to the spatial distribution of galaxies in both subsamples is the adaptive kernel density contour map (Silverman 1986; Beers 1992) drawn using the galaxies in the HD sample. The adaptive kernel technique is a two-step procedure which, after applying a pilot smoothing to estimate the local density of galaxies, uses a smoothing window the size of which decreases with increasing local density, so the statistical noise in low-density regions can be suppressed without oversmoothing the high-density ones. Two noticeable subclumps can be seen in the figures, the loca-

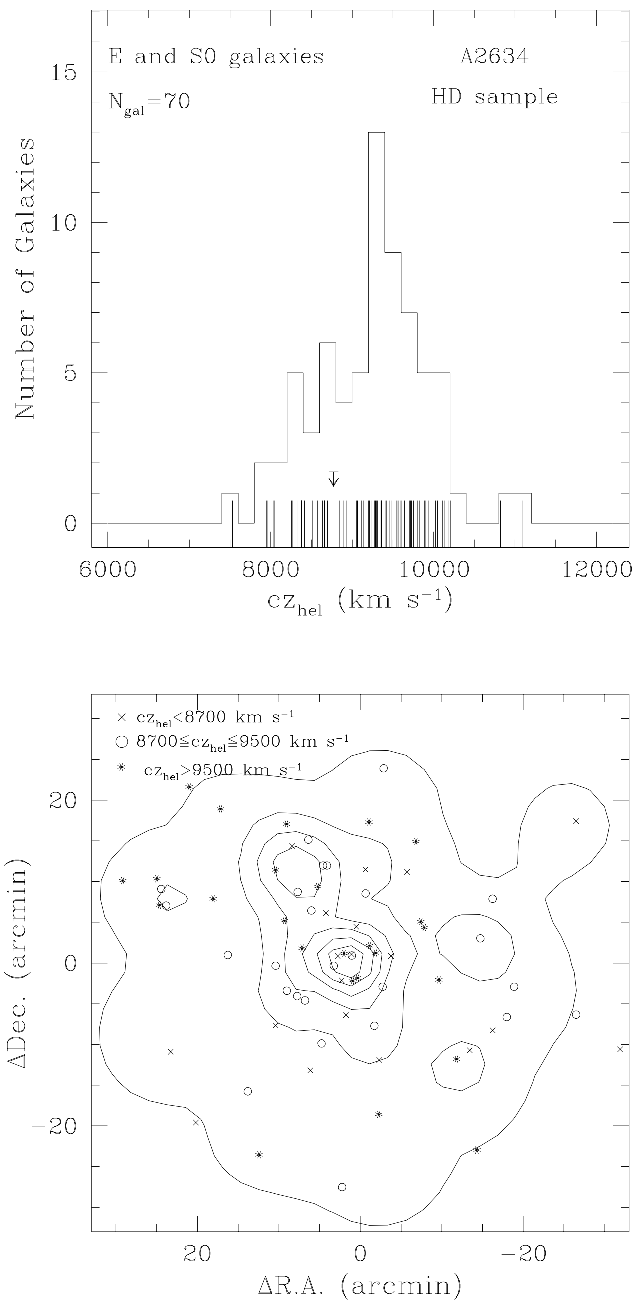

Figure 2.8 (a) Stripe density plot and velocity histogram of the early-type galaxies in the HD sample. (b) Spatial distribution of the galaxies in this subsample. Crosses identify galaxies with $cz_{hel} < 8700$ km s^{-1}, open circles galaxies with $8750 \leq cz_{hel} \leq 9500$ km s^{-1}and asterisks those with $cz_{hel} > 9500$ km s^{-1}. Solid lines are equally spaced contours of the adaptive kernel map drawn from the galaxies in the HD sample.

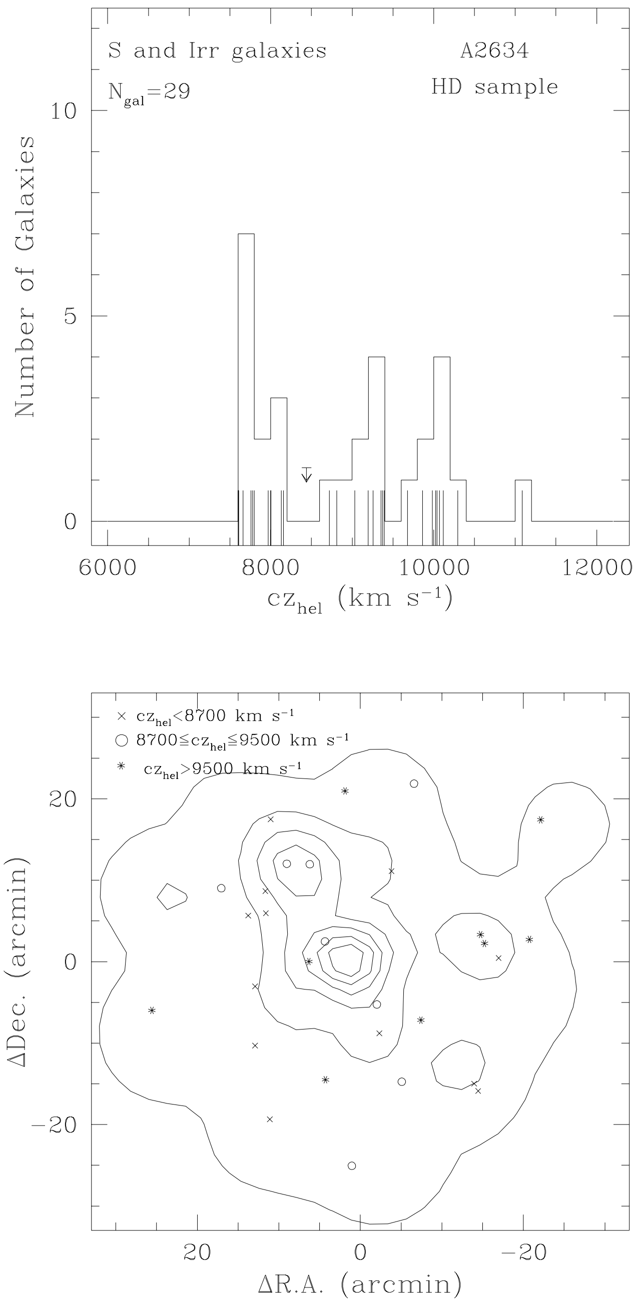

Figure 2.9 Same as in the previous figure, but for the late-type galaxies in the HD sample.

Table 2.2 Kinematic Properties of A2634

Sample	N_{gal}	V_{hel} km s^{-1}	σ km s^{-1}	M_{VT} $10^{14}M_\odot$	M_{PM} $10^{14}M_\odot$
TD All	200	9249(+55,−56)	716(+48,−35)	9.7±2.2	12.8±2.9
TD E+S0	96	9276(+67,−73)	658(+62,−42)	6.5±1.5	10.0±3.5
TD S+Irr	68	9092(+99,−126)	800(+78,−71)	15.2±3.5	14.6±4.7
HD-All	99	9151(+84,−91)	800(+61,−52)	7.5±1.7	9.9±3.1
HD-E+S0	70	9240(+79,−89)	661(+74,−52)	5.2±1.0	6.3±2.1
HD-S+Irr	29	8897(+206,−246)	1030(+116,−86)	12.8±5.2	16.8±9.1

tion of the secondary subclump being consistent with the northeast elongation seen in the X-ray image of Pinkney *et al.* (1993). To check if the apparent substructures seen in the density map correspond to kinematically different subunits, we have used different symbols for the galaxies according to three velocity ranges: 7000–8700 (crosses), 8700–9500 (circles) and 9500–11,500 km s^{-1} (asterisks). In both the early- and late-type subsamples the velocities of the galaxies are totally independent of their sky positions.

The results of the kinematical analysis presented in this section for all the different samples are summarized in Table 2.2. The name of the subsample considered is listed in column (1), and the number of galaxies in the sample is in column (2). Columns (3)–(6) list the heliocentric systemic velocity V_{hel}, the dispersion σ and their associated 68% bootstrap errors. Columns (7) and (8) give the mass estimate obtained using the different samples, as discussed in section 2.3.6.

The above results suggest that the early- and late-type galaxy populations of the HD sample have indeed very different spatial and kinematical properties (a two-sided KS test gives a probability of only 1% that a difference as large, or larger, than the one observed between the two velocity distributions can occur by chance). The spatial and kinematical distributions of velocities of early-type galaxies are compatible with them being dynamically relaxed. On the other hand, the absence of spatial segregation among the different kinematical subunits of the late-type population and their narrow velocity dispersions, suggest that this kinematical multimodality is more the signature of the infall of individual galaxies or small groups onto the cluster taking place mainly along the line-of-sight than that of a recent merger with a dispersed subcluster moving in the plane of the sky. It is also interesting to note that the correlation between velocity dispersion and X-ray temperature in clusters of galaxies recently published by Lubin & Bahcall (1993), predicts a velocity dispersion for A2634 of 690 ± 140 km s^{-1}, very close to the value derived here for the early-type subsample. Accordingly, we adopt the values of the velocity centroid and dispersion of the early-type population in the HDR sample, i.e., 9240 ± 84 km s^{-1} and 661 ± 63 km s^{-1}, respectively (here the quoted uncertainties correspond to the average of the 68% bootstrap errors), as representative of the whole cluster. Note that these values are in excellent agreement with those obtained by Pinkney *et al.* (1993) for their restricted sample of 88 galaxies free from substructure and spatial/kinematical outliers.

2.3.5 Analysis of Substructure

Both the density contours obtained via the adaptive kernel method and the shape of the velocity histograms (specially that of the late-type population) suggest the existence of substructure in the inner regions of A2634. We ascertain the statistical significance of such apparent substructure with the application of specifically designed tests.

We first consider the test developed by Salvador-Solé et al. (1993a; hereinafter referred to as the SSG test), which has been shown to be well suited for the detection of small-scale substructure in systems with circular or elliptical self-similar symmetry and with a small number of particles. Let s be the projected radial distance from the center of symmetry of a (circularly symmetrized) cluster and $N(s)$ the projected number density profile of galaxies. The SSG test produces two different estimates of $N(s)$: $N_{dec}(s)$ and $N_{dir}(s)$, which are, respectively, sensitive and insensitive to the existence of correlation among galaxy positions relative to the cluster background density; the difference among the two is interpreted as an index of existence of substructure. The estimate $N_{dec}(s)$ is obtained by inverting ("deconvolution method") the relation:

$$\Sigma(s) = \pi s (N_{dec} * N_{dec})(s) \ , \tag{2.4}$$

where $\Sigma(s)\delta s$ is the number of pairs of galaxies with observed separation between s and $s + \delta s$, among the $N_{gal}(N_{gal} - 1)/2$ pairs obtained from the N_{gal} galaxies in the cluster sample. $(N_{dec} * N_{dec})(s)$ is the autocorrelation of $N_{dec}(s)$, which, for a radially symmetric function is also equal to its self-convolution. The estimate $N_{dir}(s)$ is obtained by inverting ("direct method") the relation:

$$\Pi(s) = 2\pi s N_{dir}(s) \ , \tag{2.5}$$

where $\Pi(s)\delta s$ is the number of galaxies at projected distances between s and $s + \delta s$ from the center of symmetry of the galaxy distribution. Contrary to N_{dec}, N_{dir} does not rely on the relative separations of galaxies, therefore it is insensitive to the existence of correlation in galaxy positions. In practice, in order to use the full positional information in the data, the inversion of equations (2.4) and (2.5) relies on the cumulative forms $\int_s^\infty \Sigma(x)\,dx$ and $\int_s^\infty \Pi(x)\,dx$, rather than the distributions $\Sigma(s)$ and $\Pi(s)$ themselves, so that

$$N_{dec}(s) = \mathcal{F}_1 \circ \mathcal{A}\Big[\mathcal{A} \circ \mathcal{F}_1^{-1}\Big(2\int_s^\infty \Sigma(x)\,dx\Big)\Big]^{1/2} \ , \tag{2.6}$$

and

$$N_{dir}(s) = \mathcal{F}_1 \circ \mathcal{A}\Big[\mathcal{A} \circ \mathcal{F}_1^{-1}\Big(\int_s^\infty \Pi(x)\,dx\Big)\Big] \ , \tag{2.7}$$

where $\mathcal{F}_1$ and $\mathcal{A}$ stand, respectively, for the one-dimensional Fourier and Abel transformations (Bracewell 1978), and where the symbol "$\circ$" denotes the composition of functions. Before we proceed further, a caveat is necessary. The profile N_{dec} cannot be inferred with an arbitrarily high spatial resolution. Because the observables are not continuous functions, radial symmetry is always broken at small enough scales. This causes the argument of the square root in eq. (2.6) to take negative values due to statistical fluctuations, which requires that we filter out the highest spatial frequencies.

This results in a final N_{dec} profile convolved with a hamming window of smoothing size λ_{min} corresponding to the minimum resolution-length that guarantees the fulfillment of the radial symmetry condition. Although this additional smoothing is unnecessary for $N_{dir}(s)$, it must be also applied in order not to introduce any bias in the subsequent comparison of the two profiles.

The significance of substructure is estimated from the null hypothesis that $N_{dec}(s)$ arises from a Poissonian realization of some unknown spatial distribution of galaxies that led to *the observed distribution* of radial distances. The probability of this being the case is calculated by means of the statistic

$$\chi^2 = \frac{(N_{dec}(0) - N_{dir}(0))^2}{2S^2(0)} , \tag{2.8}$$

for one degree of freedom. In eq. (2.8), $N_{dec}(0)$ and $N_{dir}(0)$ are the values of profiles N_{dec} and N_{dir} at $s = 0$. $S^2(s)$ is the radial run of the variance of the N_{dir} profiles of 100 simulated clusters convolved to the same resolution-length λ_{min} of the observed profile. These simulated clusters are generated by the azimuthal scrambling of the observed galaxy positions around the center of symmetry of the cluster, i.e., by randomly shuffling between 0 and 2π the azimuthal angle of each galaxy, while maintaining its clustercentric distance s unchanged.

Figure 2.10a shows the projected density profiles N_{dec} and N_{dir} and their associated standard deviations for the galaxies in the circularized HD sample. It is readily apparent from this figure that both profiles are equal within the statistical uncertainties; this is confirmed by the inference from equation (2.8) that the probability that the two profiles are the same is 60%. The resulting minimum resolution-length of 0.27 Mpc puts an upper limit to the half-coherence length of any possible clump that may remain undetected in the central regions of A2634. Notice that this value is much lower than the typical value of 0.6 Mpc inferred by Salvador-Solé, Gozález-Casado, & Solanes (1993b) for the scale-length of the clumps detected in the Dressler & Shectman (1988a) clusters.

Another useful estimate of the significance of subclustering is that proposed by Salvador-Solé et al. (1993b; hereinafter referred to as the SSGS test), which can be considered a modification to the SSG test and is based on the density in excess of neighbors from a random galaxy in a cluster. The quantity

$$N_{gal}^{-1}(N_{dir} * N_{dir})(s)\bar{\xi}(s) , \tag{2.9}$$

represents the probability in excess of random of finding one cluster galaxy at an infinitesimal volume δV located at a distance s from a random cluster galaxy, per unit volume. In eq. (2.9), the "average two-point correlation function" statistic $\bar{\xi}(s)$, a generalization for isotropic but inhomogeneous systems of the usual two-point correlation function, is given by the expression:

$$\bar{\xi}(s) = \frac{(N_{dec} * N_{dec})(s) - (N_{dir} * N_{dir})(s)}{(N_{dir} * N_{dir})(s)} , \tag{2.10}$$

with

$$(N_{dec} * N_{dec})(s) = \mathcal{F}_1 \circ \mathcal{A}\Big[\mathcal{A} \circ \mathcal{F}_1^{-1}\Big(2\int_s^\infty \Sigma(x)\,dx\Big)\Big] , \tag{2.11}$$

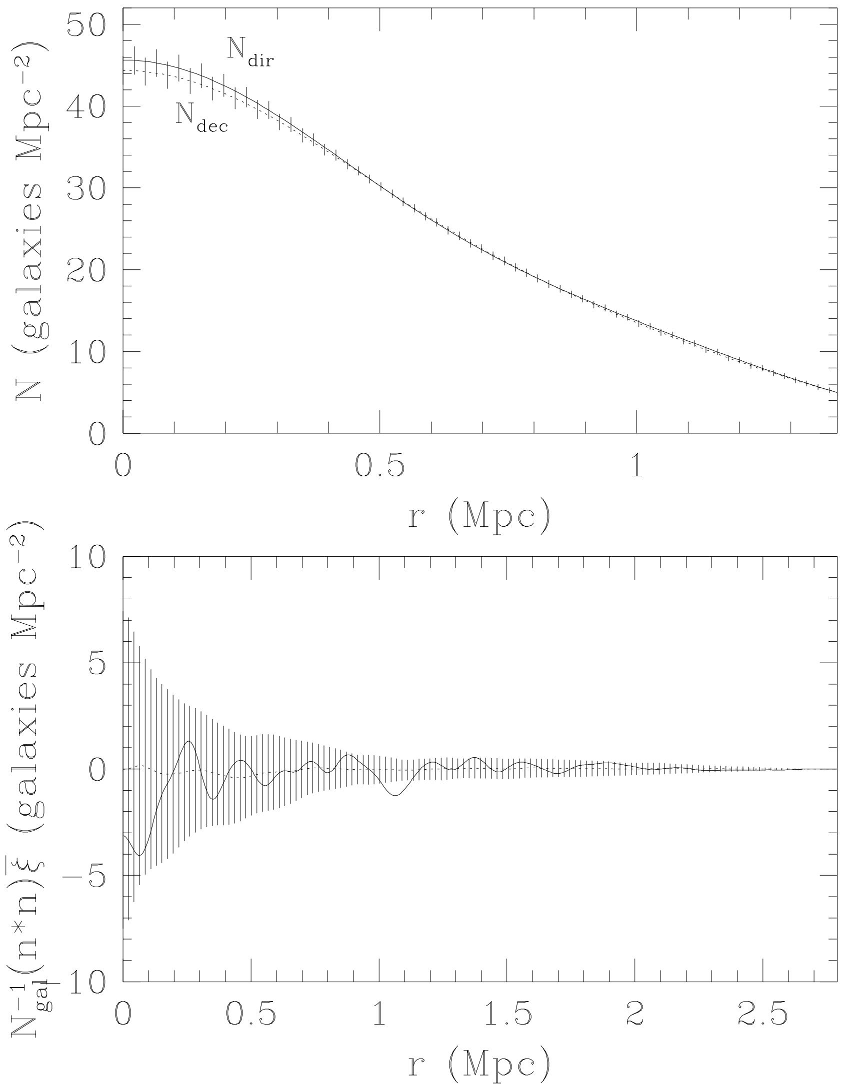

Figure 2.10 Results of the spatial tests for substructure. (a) The SSG test: projected number density profiles N_{dec} (dashed line) and N_{dir} (solid line) of the galaxies in the HD sample; vertical bars give an estimate of the 1σ-error of these profiles (see text). (b) The SSGS test: density in excess of neighbors from a random cluster galaxy for the HD sample compared with the mean value (dashed line) and 1σ-error (vertical solid lines) of this function.

and

$$(N_{dir} * N_{dir})(s) = \mathcal{F}_1 \circ \mathcal{A}\Big[\mathcal{A} \circ \mathcal{F}_1^{-1}\Big(\int_s^\infty \Pi(x)\,dx\Big)\Big]^2 . \qquad (2.12)$$

In this case, the statistical significance of substructure is obtained by checking the null hypothesis that $N_{dec}(s)$ arises from a Poissonian realization of some unknown spatial distribution of galaxies, which is approximated by $N_{dir}(s)$. In practice, the presence of substructure is estimated by the comparison of the empirical function given by eq. (2.9) with the mean and one standard deviation of the same function obtained from a large number of Poissonian cluster simulations (i.e., both the radius and the azimuthal angle of each galaxy are chosen at random) that reproduce the profile $N_{dir}(s)$. In the SSGS test, the use of Poissonian simulations, instead of angular scramblings, to estimate the statistical uncertainties translates in a partial loss of sensitivity in the detection of substructure when compared with the SSG test (see Salvador-Solé et al. 1993b for further details). This is compensated, however, by the fact that the two functions $N_{dec} * N_{dec}$ and $N_{dir} * N_{dir}$ (equations [2.11] and [2.12], respectively) can be inferred with any arbitrarily high spatial resolution, so there are no lower limits in the size of the clumps that can be detected, as opposed to the SSG test. Figure 2.10b shows the density in excess of neighbors (equation [2.9]) for the galaxies in the circularized HD sample, calculated between its center and twice its maximum radius. The dashed line and the vertical solid lines represent, respectively, the mean value of this function and its 1σ-error calculated from 200 Poissonian simulations. A low-passband hamming filter leading to a resolution length of 0.05 Mpc has been applied to attenuate the statistical noise at galactic scales. As the "signal" is embedded in the "noise", it is clear from this figure that the SSGS test does also not detect any significant substructure in the HD sample. Notice that both the SSG and the SSGS tests detect substructure in 50% of the Dressler & Shectman clusters (Salvador-Solé et al. 1993a,b).

The Dressler & Shectman (1988b) statistical test (hereinafter referred to as the DS test) complements the above spatial correlation tests because it is sensitive to kinematical substructure in the form of significant local deviations from the global distribution of radial velocities. The DS test is based on the comparison of the local velocity mean, $\bar{V}_{local}$, and velocity dispersion, σ_{local}, associated with each galaxy with measured radial velocity (calculated using that galaxy and its 10 nearest projected neighbors with measured velocities) with the mean velocity, $\bar{V}$, and velocity dispersion, σ, of the entire sample. For each galaxy, the deviation from the global values is defined by

$$\delta^2 = \frac{11}{\sigma^2}[(\bar{V}_{local} - \bar{V})^2 + (\sigma_{local} - \sigma)^2] . \qquad (2.13)$$

The observed cumulative deviation Δ_{obs}, defined as the sum of the δ's for all the galaxies with measured radial velocities, is the statistic used to quantify the presence of substructure. To avoid the formulation of any hypothesis on the form of the velocity distribution of the parent population, this statistic is calibrated by Monte-Carlo simulations that randomly shuffle the velocities of the galaxies while keeping fixed their observed positions. In this way any existing correlation between velocities and positions is destroyed. The significance of subclustering is then given in terms of the fraction of simulated clusters for which their cumulative deviation Δ_{sim} is larger than Δ_{obs}.

A visual judgment of the statistical significance of local deviations from the global kinematics for the galaxies in our HD sample can be done comparing the plots in Figures

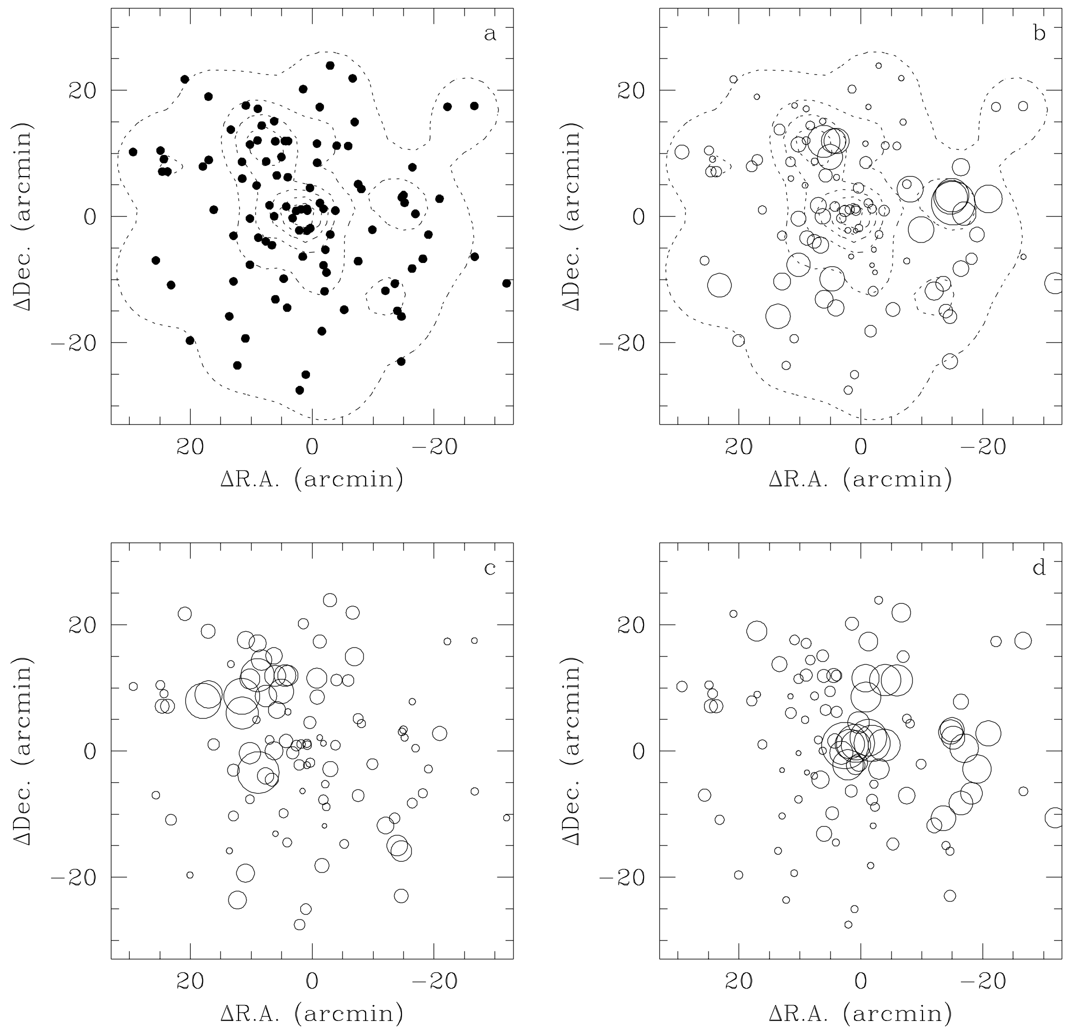

Figure 2.11 Local deviations from the global kinematics for the the galaxies galaxies in the HD sample as measured by the DS test. (a) Spatial distribution of the HD sample galaxies (filled circles) superposed on the adaptive kernel density contour map of the HD sample (dashed lines). (b) The position of galaxies are marked with open circles which radius scales with their local deviation δ from the global kinematics (see text), from which the test statistic $\Delta_{obs} = \sum \delta's$ is calculated. The adaptive kernel contour map of the HD sample is superposed (dashed lines). (c)–(d) Monte-Carlo models of the HDR sample obtained after 1000 random shufflings of the velocities of the galaxies. Panel (c) shows the model with a cumulative deviation Δ_{sim} closest to the median of the simulations. Panel (d) corresponds to the model whose Δ_{sim} is closest to the value of the upper quartile. Coordinates are measured with respect to the center adopted for A2634.

2.11a–d. Figure 2.11a shows the spatial distribution of the HD sample galaxies (filled circles) superposed on the adaptive kernel density contour map of the HD sample (dashed lines). The coordinates are measured with respect to the center adopted for A2634. In Figure 2.11b each galaxy is identified with a circle whose radius is proportional to e^{δ} (with δ given above). Hence, the larger the circle, the larger the deviation from the global values (but beware of the insensitivity of the definition of δ given by eq. [2.13] to the sign of the deviations from the mean cluster velocity). The superposition of the projected density contours (dashed lines) shows that, among the subclumps seen in the adaptive kernel map, the small density enhancement at plot coordinates (-15,3), and to a lesser extent the density enhancement at (8,12), are related with apparently large local deviations from the global kinematics. The remaining figures show two of the 1000 Monte-Carlo models performed: Figure 2.11c corresponds to the one whose Δ_{sim} is closest to the median of the Δ's of all the simulations, while Figure 2.11d corresponds to the simulation whose Δ_{sim} is closest to the value of the upper quartile. The comparison of Figure 2.11b with these last two figures reveals that the observed local deviations from the global kinematics in the HD sample are indeed statistically insignificant. This is corroborated by the fact that the value of Δ_{sim} is larger than Δ_{obs} in more than 71% of the Monte-Carlo models. Even if we run the same test for the subset of late-type galaxies the value of Δ_{sim} is still larger than Δ_{obs} in the 57% of the simulated clusters.

Based on the results of the above spatial and kinematical analysis, we consider the apparent clumpiness of the central regions of A2634 seen in the kernel map as statistically insignificant (i.e., consistent with Poissonian fluctuations of the galaxy distribution). The kinematical test has also provided quantitative confirmation of the fact that the velocities of the late-type population are not segregated in the plane of the sky, although we cannot exclude the possibility that an important fraction of the spirals is located in loose groups superposed along the line-of-sight.

2.3.6 Mass Estimates

The virial theorem is customarily used as the standard tool to estimate the dynamical mass of galaxy clusters. Under the assumptions that the cluster is a spherically symmetric system in hydrostatic equilibrium and that the mass distribution follows closely that of the observed galaxies independently of their luminosity, the total gravitating mass of a cluster is given by

$$M_{\rm VT} = \frac{3\pi}{G}\sigma^2 R_H \ , \tag{2.14}$$

where σ is the line-of-sight velocity dispersion of the galaxies taken here as the biweight scale estimate, and R_H is the cluster mean harmonic radius, defined as

$$R_H = \frac{D}{2} N_{gal}(N_{gal}-1)\Big(\sum_i \sum_{j<i} \frac{1}{\theta_{ij}}\Big)^{-1} \ , \tag{2.15}$$

where D is the cosmological cluster distance, θ_{ij} is the angular separation between galaxies i and j, and N_{gal} the total number of galaxies.

An alternative approach is to use the "projected mass estimator" (Bahcall & Tremaine 1981; Heisler, Tremaine, & Bahcall 1985)

$$M_{\rm PM} = \frac{32}{\pi G N_{gal}} \sum_i V_i^2 R_i \ , \tag{2.16}$$

where V_i is the observed radial component of the velocity of galaxy i with respect to the systemic velocity of the cluster, and R_i is its projected separation from the cluster center. The numerical factor in front of eq. (2.16) assumes an isotropic distribution of galaxy orbits. It is worth noting that the cluster masses obtained with these two methods may underestimate the actual ones if the distribution of matter is less concentrated than the light.

Mass estimates using the above two methods and their 68% uncertainties (computed by means of the bootstrap technique and a standard propagation of errors analysis) are listed in columns (7) and (8) of Table 2.2, for the TD and HD samples. In addition, because of the clearly different spatial and kinematical properties shown by the early- and late-type galaxies of A2634, we have also derived mass estimates for the two populations. We can compare the different mass estimates for the HD sample given in Table 2.2 with the value of $2.5 \times 10^{14}\,M_\odot$ calculated for the central cluster region from the observed X-ray gas distribution (Eilek et al. 1984). The better agreement is obtained with the mass estimates inferred for the early-type population, while the late-type galaxies yield excessively large values. This result adds further support to the idea, discussed in section 2.3.4, that the spiral galaxies of A2634 represent a young cluster population, not yet in a relaxed dynamical state, and possibly with a different distribution of orbits than the early-type galaxies. A similar difference between the mass estimates of the early- and late-type galaxies is also present in the TD sample. Note that if the spiral galaxies were all falling onto the cluster along purely radial orbits, their average velocity would be on the order of $\sqrt{2}$ times the mean velocity of the relaxed cluster population. This higher velocity would produce an overestimate of the cluster mass by a factor of two, very close to the observed difference between the mass estimates of the early- and late-type populations.

On the other hand, a rough estimate of the radius of the virialized region for a typical rich cluster (Maoz 1990) gives $r_{vir} = 2.48\,\mathrm{Mpc}$, which corresponds to 0.8^o at the distance of A2634. This suggests that even some of the early-type galaxies in the TD sample might be part of an unrelaxed population. Consequently, we adopt as the best estimate of the virial mass of A2634 that given by the early-type population of the HD sample.

2.3.7 Conclusions

An extensive galaxy redshift survey around A2634 serves to reveal a region of intricate topology at all scales. Besides the large-scale structure associated with the PPS, we are able to identify in the 6^o wide field around A2634 several clusters and groups: (a) A2634; (b) A2666; (c) two rich and massive background clusters, also detected in the X-ray domain, located at respectively twice and four times the redshift of A2634; and (d) two spiral rich groups near A2634 at ~ 7500 and $\sim 11{,}500$ km s^{-1}, respectively.

The dynamical complexity of this region is also reflected in the structure of the best sampled of its galaxy concentrations: A2634. While the spatial, kinematical and dynamical properties of the early-type population agree fairly well with those expected for a relaxed system, the spiral galaxies are not only less concentrated to the cluster core, but they also display strong evidence for multimodality in their velocity distribution and dominate the high-velocity tails, suggesting their recent arrival to the cluster. In addition, spirals are virtually absent from the central parts of A2634, a result similar to that obtained by Beers et al. (1992) for A400. These results have two important implications. First, the velocity centroid of the (presumably virialized) innermost cluster region can be miscalculated and/or its velocity dispersion overestimated if (asymmetric) secondary infall plays an important role. It is therefore advisable to use only the early-type galaxy population to derive these two properties. Based on this consideration, we advocate the following choice of parameters for A2634: systemic velocities of 9240 km s^{-1}, velocity dispersions of 661 km s^{-1}, and virial mass of $5.2 \times 10^{14}\,M_{\odot}$. Second, unless secondary infall is a recent event in the life of these clusters, late-type newcomers must be efficiently converted into early-type systems in order to explain the scarcity of the former types in the innermost cluster regions.

The clumpiness shown by the galaxy number density map of the central regions of A2634 and the multimodal velocity distribution of the late-type population, are investigated as possible signatures of a recent collision of this cluster with a large subunit. Statistical tests for substructure find, however, no significant evidence of clumpiness in the galaxy component of A2634 that can corroborate the occurrence of a merger in the plane of the sky, but we cannot exclude the existence of smaller, loose groups of spirals, unlikely associated with dense ICMs, spatially superposed. This result indicates that the structure and kinematics of A2634 reflect the continuous infall of individual galaxies or small groups onto the cluster along the line-of-sight, rather than the recent merger of two comparable subunits moving in the plane of the sky.